This article has been accepted for publication in IEEE Signal Processing Letters. This is the author's version which has not been fully edited and content may change prior to final publication. Citation information: DOI 10.1109/LSP.2026.3724106

IEGC-FSDN: Foggy Ship Detection Network with Integrating Edge and Global Constraints

Yi Yang, Yu Wan, Jie Li, *Member, IEEE*, Liupeng Lin, Zaiyan Zhang

***Abstract*—With advances in aerial technology, remote-sensing object interpretation has found ubiquitous applications across diverse domains. Owing to atmospheric interference, haze severely degrades the quality of optical remote sensing images—an effect that is particularly pronounced over water, where evaporative moisture frequently produces dense fog in harbors and open-sea scenes. Consequently, ship detection under hazy conditions has become an extremely challenging task. To address this issue, we propose a Foggy Ship Detection Network with Integrating Edge and Global Constraints (IEGC-FSDN). The network introduces a Progressive Restoration Strategy that simultaneously leverages edge and global constraints to progressively recover haze-corrupted features within the detector, thereby enhancing the model's perceptual capacity for ships in fog. In addition, a Multi-Scale Atmospheric Prior Module (MSAPM) is embedded to explicitly incorporate atmospheric physical priors, further strengthening robustness. The experimental results demonstrate that IEGC-FSDN achieves superior performance compared to state-of-the-art alternatives, with only a marginal increase in parameters over the baseline. The code is released at: https://github.com/KIKYOUWY/IEGC-FSDN.**

***Index Terms*—Ship object detection, Foggy weather, Edge and global constraints.**

I. INTRODUCTION

DUE to the high moisture content over the sea surface, fog frequently appears in offshore areas and harbors, degrading remote-sensing image quality and weakening the semantic and fine-grained cues required for ship detection. Existing foggy-object detection methods can be broadly grouped into direct, distributed, and union strategies [1], [2]. Direct methods [3], [4] train detectors on foggy images, but degraded supervision limits representation learning. Distributed methods [5]–[9] first restore images and then detect objects; recent dehazing works further explore semi-supervised multi-prior/domain-transfer learning and weakly supervised physics-based decomposition [15], [16], together with diffusion priors, global-context tokenization, restoration backbones, detail attention, and real-image adaptation [17]–[21]. However, visually optimized restoration does not necessarily improve ship localization. Union methods [22]–[25] jointly optimize restoration and detection, but they mainly enhance global feature clarity and still insufficiently model edge/detail restoration across object scales. Recent remote-sensing studies address small ships, haze, class imbalance, drone-view haze, and low-quality imaging [26]–[32], while progressive edge/global restoration for foggy ship detection remains underexplored. To address these limitations, we propose IEGC-FSDN, a foggy ship detection network integrating edge and global constraints. A Progressive Restoration Strategy imposes local edge supervision on high-resolution stages and global constraints on low-resolution stages, enabling scale-aware refinement of haze-corrupted features. Meanwhile, a Multi-Scale Atmospheric Prior Module (MSAPM) injects physics-inspired atmospheric priors into detection features to improve haze robustness. The main contributions are twofold: (1) a progressive edge/global restoration strategy is designed to preserve fine structures and contextual consistency across feature scales; and (2) MSAPM embeds multi-scale atmospheric priors into the detector, guiding haze-invariant feature learning and improving foggy ship detection accuracy.

Y. Yang is the School of Intelligent Sports Engineering, Wuhan Sports University, Wuhan 430079, China (e-mail: yyi@whsu.edu.cn).

Y. Wan and Z. Zhang are with the School of Geodesy and Geomatics, Wuhan University, Wuhan 430079, China (e-mail:2024282140091@whu.edu.cn,zzaiyan@whu.edu.cn,).

L. Lin is with the School of Resource and Environmental Sciences, Wuhan University, Wuhan 430079, China (e-mail: linliupeng@whu.edu.cn).

J. Li is with the School of Geodesy and Geomatics, Wuhan University, Wuhan 430079, China, and is also with Hubei Luojia Laboratory, Wuhan 430079, China.(e-mail: jli89@sgg.whu.edu.cn). (Corresponding author: Yu Wan.).

II. THE PROPOSED METHOD

A. Architecture of the Proposed Method and Progressive Restoration Strategy

Architecture of IEGC-FSDN: The inadequate utilization of multi-scale features in current works severely hinders the detection of small targets in foggy environments. To bridge this gap, we present the IEGC-FSDN, a specialized architecture illustrated in Fig. 1. Unlike the heavy computational burden of traditional baselines, our method adopts a highly parameter-efficient design. It incorporates a Progressive Restoration Strategy to enforce edge and global constraints, and seamlessly integrates a Multi-Scale Atmospheric Prior Module (MSAPM) to enhance feature robustness.

During inference, the network architecture maintains the standard pipeline of the baseline. The input is propagated through a Stem pre-processing layer followed by the Res2–Res5 stages to generate hierarchical feature representations. These multi-scale features are then aggregated via a Feature Pyramid Module (FPM) [34] and transmitted to the detection head—implemented using DiffusionDet [35] to yield the final bounding box predictions.

Multi-Scale Atmospheric Prior Module: Unlike the baseline, we insert the Multi-Scale Atmospheric Prior Module (MSAPM) after the Stem, Res2, and Res3 stages, strengthening robustness and the network's sensitivity to fog-degraded target features.

A Progressive Restoration Strategy that leverages edge and global constraints: We propose a Progressive Restoration

This article has been accepted for publication in IEEE Signal Processing Letters. This is the author's version which has not been fully edited and content may change prior to final publication. Citation information: DOI 10.1109/LSP.2026.3724106

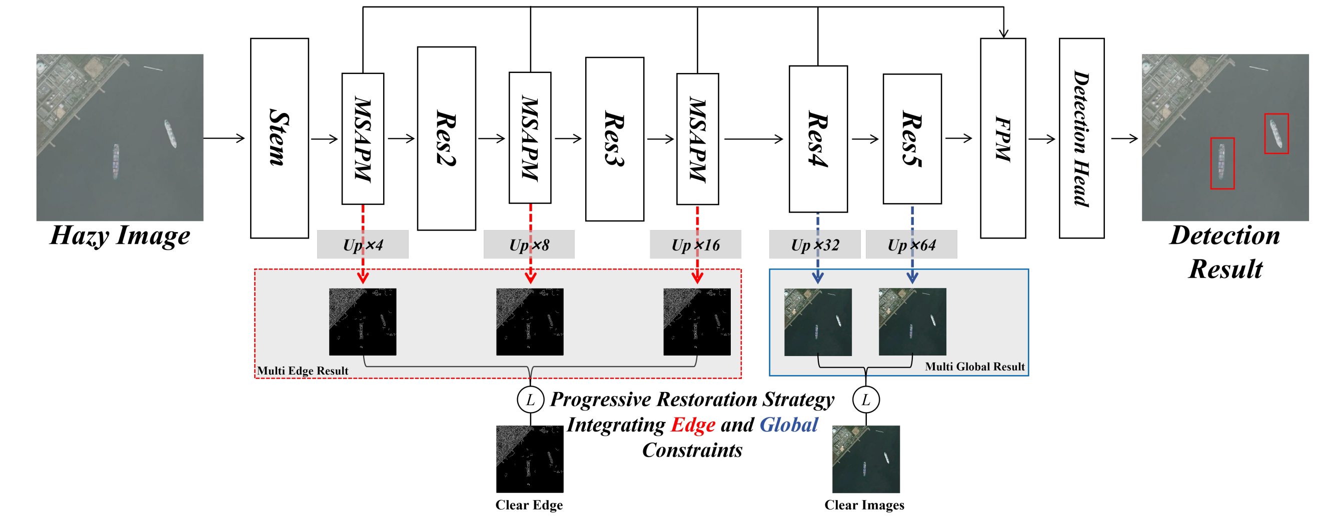

Fig. 1. Overall architecture of the proposed IEGC-FSDN.

Strategy that hierarchically embeds edge and global constraints to capture ship features of varying scales. Furthermore, by distributing supervision signals, it alleviates the vanishing gradient problem typically associated with supervising a deep architecture via a solitary restoration loss. Given that the feature maps of the first three stages (Stem, Res2, and Res3) retain a large spatial resolution, we construct a local edge dehazing loss to emphasize fine structural details by minimizing the discrepancy between the intermediate restored outputs and the ground-truth images. Conversely, Res4 and Res5 produce smaller-scale features that encode global context; hence, a global dehazing loss is proposed to regularize these semantically richer but spatially coarser representations. In the aforementioned five stages, the feature maps from different levels are projected and upsampled back to the original input size. We then employ either the local edge loss or the global loss to progressively optimize the feature representation at each specific scale. The upsampling operation for each layer can be formulated as follows:

$$I_{\text{Upout}} = f_{\text{Up}}\left(f_{\text{PC}}\left(f_{\text{DSC}}\left(F_{\text{Upinput}}\right)\right)\right). \tag{1}$$

where I_{Upout} and F_{Upinput} are the output and input of the upsampling layer, respectively. The functions $f_{\text{DSC}}(\cdot)$, $f_{\text{PC}}(\cdot)$, and $f_{\text{Up}}(\cdot)$ represent the depthwise separable convolution, pointwise convolution, and pixel shuffle layer, respectively.

Utilizing this lightweight upsampling mechanism, multi-scale features from the backbone are spatially aligned with the original input resolution. This facilitates direct pixel-level supervision against the clean reference images.

B. Multi-Scale Atmospheric Prior Module

To enhance the perceptual capacity and robustness of the detection model for objects under foggy conditions, we propose the Multi-Scale Atmospheric Prior Module (MSAPM) and integrate it after the Stem, Res2, and Res3 layers. Its architecture is illustrated in Fig. 2.

The Multi-Scale Atmospheric Prior Module incorporates prior knowledge from the atmospheric transmission model to enhance the model's generalization and robustness. The atmospheric transmission model can be expressed as:

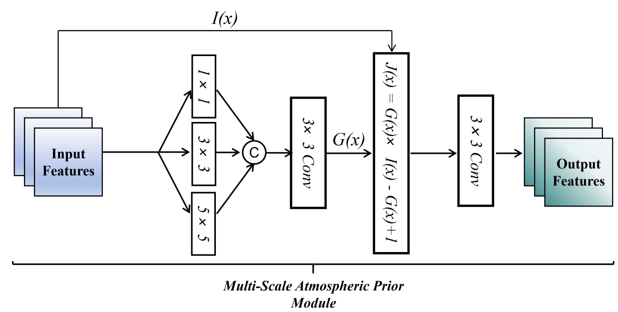

Fig. 2. Structure of the Multi-Scale Atmospheric Prior Module (MSAPM).

$$I(x) = J(x)t(x) + A\left(1 - t(x)\right). \tag{2}$$

where $I(x)$ denotes the degraded image, $J(x)$ denotes the clear image, $t(x)$ represents the transmission map, and A denotes the global atmospheric light. Following AOD-Net [8], we algebraically combine $t(x)$ and A into a new variable $G(x)$; the transformed equation becomes:

$$J(x) = G(x) \cdot I(x) - G(x) + b. \tag{3}$$

where $G(x)$ is the unified variable obtained by merging A and $t(x)$, and b is a bias term set to 1 in this work. Through this transformation, the model only needs to learn $G(x)$. The acquisition of $G(x)$ can be expressed as:

$$\begin{aligned} G(x) = f_{\text{Conv3}}\Big(&f_{\text{Cat}}\left(f_{\text{Conv4}}(F_D), f_{\text{Conv5}}(F_D),\right.\\ &\left.f_{\text{Conv6}}(F_D)\right)\Big). \end{aligned} \tag{4}$$

where $f_{\text{Conv3}}(\cdot)$ denotes a $3{\times}3$ convolution for channel adjustment, $f_{\text{Cat}}(\cdot)$ denotes the concatenation operation, $f_{\text{Conv4}}(\cdot)$, $f_{\text{Conv5}}(\cdot)$, and $f_{\text{Conv6}}(\cdot)$ denote multi-scale convolutions with kernel sizes 1×1, 3×3, and 5×5, respectively. F_D denotes the input detection features. Subsequently, the result is fed into the transformed equation as $I(x)$ to obtain $J(x)$, which serves as the output feature representation. MSAPM enhances robustness by leveraging multi-scale convolutions to extract detection features and embedding prior knowledge derived from the atmospheric scattering model. Different from AOD-Net, which performs image-level restoration, MSAPM applies the transformed atmospheric prior to intermediate detection features. The parallel 1×1, 3×3, and 5×5 convolutions provide receptive fields of different sizes, enabling the module to enhance small ships with local structural cues and larger ships with broader contextual responses. Moreover, inserting MSAPM into multiple backbone stages introduces atmospheric-prior guidance into hierarchical feature learning, which is more suitable for remote-sensing ship detection with large object-scale variations.

C. Union Loss of Leveraging Edge and Global Constraints

To achieve superior robustness and detection accuracy in adverse weather, we formulate a composite objective function that jointly optimizes the detection and dehazing tasks:

$$L_{\mathrm{Total}} = L_{\mathrm{DH}} + L_{\mathrm{OD}}. \tag{5}$$

where L_{Total} is the total multi-task union loss, L_{DH} is the dehazing loss, and L_{OD} is the object detection loss. The dehazing function L_{DH} is derived from the proposed Progressive Restoration Strategy, explicitly integrating edge and global constraints. The overall dehazing function is formulated as a combination of local edge and global components. During the initial three stages, we impose a local edge dehazing loss specifically designed to restore the fine-grained structural details of small objects encoded in the high-resolution feature maps. For the latter two stages, we impose a global restoration constraint. Specifically, a global dehazing loss optimizes the network to restore global atmospheric consistency from the low-resolution, yet semantically robust representations. The global dehazing loss is formulated as:

$$L_{\mathrm{GD}} = \frac{1}{N}\sum_{i=1}^{N}\sqrt{\left(I^{i}_{\mathrm{Upout}} - I^{i}_{\mathrm{label}}\right)^2 + \varepsilon^2}. \tag{6}$$

where I_{label} represents the clear labels, N represents the number of training samples, and ε is a small positive constant added to prevent numerical instability and smooth the optimization process. In this work, ε is set to 10^{-3}. Edges are extracted from both the upsampled output I_{Upout} and the clear label I_{label}, and the structural divergence between the reconstructed and ground-truth edge maps is penalized. This mechanism explicitly enhances the model's sensitivity to fine-grained details of small objects preserved within the high-resolution feature maps. The process of extracting the edge features and the local edge dehazing loss L_{LED} can be expressed as follows:

$$F_{\mathrm{edge}} = I - k_{\mathrm{gauss}} \cdot f_{\mathrm{up}}\left(f_{\mathrm{down}}\left(k_{\mathrm{gauss}} \cdot I\right)\right). \tag{7}$$

$$L_{\mathrm{LED}} = \frac{1}{N}\sum_{i=1}^{N}\sqrt{\left(F^{i}_{\mathrm{edgeup}} - F^{i}_{\mathrm{edgelabel}}\right)^2 + \varepsilon^2}. \tag{8}$$

where F_{edge} represents the extracted edge features, I represents the original images, and k_{gauss} is a Gaussian kernel. In addition, $f_{\mathrm{up}}(\cdot)$ and $f_{\mathrm{down}}(\cdot)$ denote upsampling and downsampling, respectively. Leveraging a progressive local edge and global constraint strategy, feature representations in the backbone undergo hierarchical restoration. Specifically, high-resolution (shallow) maps are guided by local edge constraints to maintain the structural integrity of small targets, while low-resolution (deep) maps are optimized by global constraints to restore atmospheric consistency. This synergistic approach effectively enhances detection robustness across a wide range of object scales in adverse weather.

The object detection loss L_{OD} consists of three parts. The detection loss can be expressed as:

$$L_{\mathrm{OD}} = \beta_{\mathrm{focal}} L_{\mathrm{focal}} + \beta_{\mathrm{L1}} L_{\mathrm{L1}} + \beta_{\mathrm{giou}} L_{\mathrm{giou}}. \tag{9}$$

Specifically, L_{focal} denotes the focal loss, which is designed to address the class imbalance problem by focusing on hard-to-classify samples. It measures the discrepancy between the predicted and actual class labels. L_{L1} represents the L1 loss, which quantifies the difference between the estimated and actual bounding boxes. Additionally, L_{giou} is the loss based on the Generalized Intersection over Union (GIoU) metric [36], which evaluates the similarity between the estimated and actual bounding boxes. Following the default DiffusionDet configuration [35], the coefficients β_{focal}, β_{L1}, and β_{giou} are set to 2, 5, and 2, respectively, and kept unchanged for fair comparison with the baseline detector.

III. EXPERIMENTS

A. Implementation Details

All experiments were conducted using an NVIDIA GeForce GTX 4080 GPU with 16GB RAM. The model was optimized using the ADAMW optimizer [37], configured with an initial learning rate of 0.000025 and a weight decay of 10^{-4}. For data preprocessing, normalization was applied based on the standard deviations [58.395, 57.120, 57.375] and means [123.675, 116.280, 103.530] across the three channels. The number of diffusion detection boxes was set to 500. Model performance was evaluated using the mean Average Precision (mAP) metric, which assesses the precision across multiple IoU thresholds, typically ranging from 0.5 to 0.95 with increments of 0.05.

The synthetic dataset comprises a total of 14,920 training images and 4,974 testing images. It synthesizes fog-degraded images by manually augmenting ship instances collected from publicly available remote sensing object detection datasets such as DOTA [38] and HRSSD. Spatially varying transmission maps are extracted from foggy images using dark-channel and dark-object subtraction strategies, resized to 512×512, and fused with clear ship images using $\gamma = 0.6$, which controls the fog-blending strength and yields moderate, non-uniform degradation while preserving ship structures. To further verify the generalization capability of IEGC-FSDN under authentic foggy conditions, we construct a real foggy ship dataset containing 1,348 foggy remote-sensing images with a spatial size of 512×512, which will be released together with the source code. The synthetic and real data are shown in Fig. 3.

B. Comparative Experiments on Foggy Weather Detection

To validate the superiority of IEGC-FSDN, we select 14 representative competitors covering three distinct strategies, including two recent remote-sensing dehazing networks, SFRDP-Net [13] and DR3DF-Net [14], and the recent adverse-weather detector MASFNet [33]. The results are reported in Table I. The original metric columns report quantitative

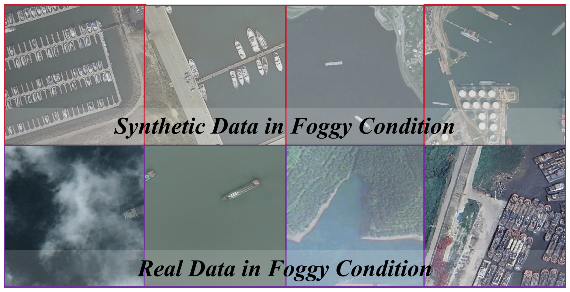

Fig. 3. Synthetic (red) and real (blue) foggy samples.

TABLE I
DETECTION RESULTS ON SYNTHETIC AND REAL FOGGY SHIP DATA

Strategy	Method	Syn. mAP	Large	Medium	Small	Real mAP
Direct	Faster R-CNN	58.905	48.0	65.3	52.9	11.862
	Sparse R-CNN	59.316	47.9	65.7	54.0	12.955
	DiffusionDet	61.183	49.6	67.9	56.5	12.612
Distributed	ACE [10]	61.548	48.7	67.5	55.2	13.857
	DCP [11]	61.799	51.3	67.7	55.1	14.127
	AOD [8]	63.084	51.3	69.7	57.5	13.567
	GridDehaze [12]	62.350	50.4	69.1	57.0	12.986
	SFRDP-Net [13]	63.901	51.8	70.8	59.5	13.788
	DR3DF-Net [14]	63.008	50.3	69.4	57.5	14.311
Union	CascadeNet	61.815	49.8	71.1	60.3	13.276
	IA-YOLO	58.285	45.6	64.6	53.2	10.481
	DSNet	63.569	44.6	68.9	57.3	12.035
	BADNet	63.763	50.9	70.5	59.3	12.298
	MASFNet	64.339	52.1	71.1	60.8	12.109
	IEGC-FSDN	**66.395**	**54.8**	**72.5**	**61.5**	**15.198**

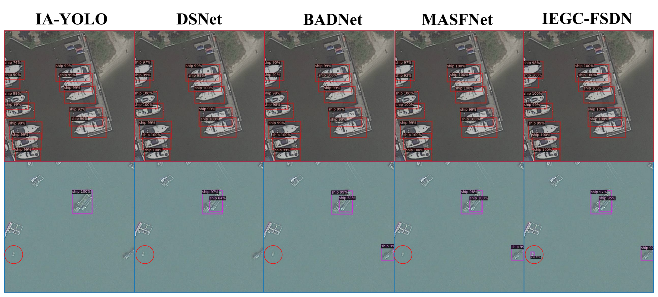

Fig. 4. Detection results on synthetic (red) and real (blue) samples.

results on the synthetic foggy ship test set, while the rightmost column reports mAP on the newly constructed real foggy ship dataset. In addition to the overall mAP, separate evaluations for large, medium and small objects are provided to demonstrate multi-scale detection capability. Since small ships rely more strongly on local contours and fine-grained details, the Small metric in Table I is used as a detection-oriented indicator of detail-sensitive perception. Experimental results show that IEGC-FSDN achieves the best overall detection performance on the synthetic test set and demonstrates practical generalization ability under authentic foggy imaging conditions. Compared with MASFNet, IEGC-FSDN improves Syn. mAP from 64.339 to 66.395 and Small performance from 60.8 to 61.5. On the real foggy ship dataset, IEGC-FSDN achieves 15.198 mAP, outperforming the best competing result by 0.887 points.

Fig. 4 shows that IEGC-FSDN produces more accurate detections with higher confidence on both synthetic and real foggy images.

C. Ablation Experiment

To further demonstrate the effectiveness of the Progressive Restoration Strategy and MSAPM, we conduct ablation studies on each component. Table II summarizes the individual and joint contributions of the two core designs. Table III shows that placing MSAPM after the first three stages yields the best trade-off among accuracy, speed, and parameter overhead.

TABLE II
COMPONENT ABLATION STUDY

Method	PRS	MSAPM	mAP	Params (M)	Speed (ms)
Baseline	–	–	61.183	129.491	30.1
PRS only	√	–	65.446	129.491	30.1
MSAPM only	–	√	63.111	129.699	33.7
Full	√	√	66.395	129.699	33.7

TABLE III
MSAPM PLACEMENT ABLATION

Method	mAP	Speed (ms)	Params (M)
Baseline*	65.446	30.1	129.491
MSAPM_Stem	65.552	32.2	129.507
MSAPM_Res2	65.803	32.7	129.571
MSAPM_Res3	66.395	33.7	129.699
MSAPM_Res4	66.071	34.7	129.954
MSAPM_Res5	66.236	35.2	130.464

Compared with the baseline, using MSAPM alone improves mAP from 61.183 to 63.111 by incorporating multi-scale atmospheric priors, while using PRS alone further improves mAP to 65.446 through hierarchical edge/global restoration. Combining both components achieves the best mAP of 66.395, indicating that physics-guided feature enhancement and progressive restoration provide complementary benefits.

D. Comprehensive Analysis of Experiments

To demonstrate that IEGC-FSDN is not only superior in accuracy but also highly efficient and lightweight, we compare its computational cost with that of the competing methods in Table IV.

The results show that IEGC-FSDN attains the best mAP with negligible overhead. It improves mAP over MASFNet from 64.339 to 66.395 while requiring smaller increments (+4 ms/+0.207M), and is more accurate and lightweight than the newly added SFRDP-Net and DR3DF-Net.

TABLE IV
EFFICIENCY ANALYSIS

Method	Speed (ms)	Params (M)	mAP
Baseline	30	129.491	61.183
ACE_baseline	+654	+0	61.548
DCP_baseline	+150	+0	61.799
AOD_baseline	+1	+0.018	63.084
GridDehaze_base	+12	+0.958	62.350
SFRDP-Net	+77	+3.510	63.901
DR3DF-Net	+154	+9.081	63.008
CascadeNet	+1	+0.018	61.815
IA-YOLO	+9	+0.558	58.285
DSNet	+0	+0	63.569
BADNet	+8	+0.788	63.763
MASFNet	+9	+0.320	64.339
IEGC-FSDN	+4	+0.207	**66.395**

IV. CONCLUSION

In this paper, we propose IEGC-FSDN, which integrates progressive edge/global constraints and MSAPM to recover fog-degraded detection features. Experiments on synthetic and real foggy ship datasets demonstrate superior detection performance with negligible additional parameters and inference overhead. Under extremely adverse conditions, infrared or other multimodal sensing may be required to achieve more robust detection.

REFERENCES

[1] C. Y. Li *et al.*, "Detection-friendly dehazing: Object detection in real-world hazy scenes," *IEEE Trans. Pattern Anal. Mach. Intell.*, vol. 45, pp. 8284–8295, 2023.

[2] Y. Wan, J. Li, L. Lin, Q. Yuan, and H. Shen, "Collaboration of dehazing and object detection tasks: A multi-task learning framework for foggy image," *IEEE Trans. Geosci. Remote Sens.*, pp. 1–1, 2025.

[3] C. Wang, C. Li, B. Luo, W. Wang, and J. Liu, "RiWNet: A moving object instance segmentation network being robust in adverse weather conditions," arXiv:2109.01820, doi: 10.48550/arXiv.2109.01820.

[4] J. Xia, T. Chen, and J. Qiao, "Vehicle detection based on YOLOv3 in adverse weather conditions," in *Proc. IEEE 4th Int. Conf. Civil Aviation Safety and Information Technology (ICCASIT)*, 2022, pp. 692–696.

[5] Y. W. Qiu *et al.*, "MB-TaylorFormer: Multi-branch efficient transformer expanded by Taylor formula for image dehazing," in *Proc. IEEE/CVF Int. Conf. Computer Vision (ICCV)*, Paris, France, 2023, pp. 12756–12767.

[6] X. Qin, Z. L. Wang, Y. C. Bai, X. D. Xie, and H. Z. Jia, "FFA-Net: Feature fusion attention network for single image dehazing," in *Proc. AAAI Conf. Artificial Intelligence*, vol. 34, New York, NY, USA, 2020, pp. 11908–11915.

[7] B. Y. Li *et al.*, "Benchmarking single-image dehazing and beyond," *IEEE Trans. Image Process.*, vol. 28, pp. 492–505, 2019.

[8] B. Y. Li, X. L. Peng, Z. Y. Wang, J. Z. Xu, and D. Feng, "AOD-Net: All-in-one dehazing network," in *Proc. IEEE Int. Conf. Computer Vision (ICCV)*, Venice, Italy, 2017, pp. 4780–4788.

[9] B. L. Cai, X. M. Xu, K. Jia, C. M. Qing, and D. C. Tao, "DehazeNet: An end-to-end system for single image haze removal," *IEEE Trans. Image Process.*, vol. 25, pp. 5187–5198, 2016.

[10] A. Rizzi, C. Gatta, and D. Marini, "A new algorithm for unsupervised global and local color correction," *Pattern Recognit. Lett.*, vol. 24, no. 11, pp. 1663–1677, 2003.

[11] K. He, J. Sun, and X. Tang, "Single image haze removal using dark channel prior," *IEEE Trans. Pattern Anal. Mach. Intell.*, vol. 33, no. 12, pp. 2341–2353, Dec. 2011.

[12] X. Liu, Y. Ma, Z. Shi, and J. Chen, "GridDehazeNet: Attention-based multi-scale network for image dehazing," in *Proc. IEEE/CVF Int. Conf. Comput. Vis. (ICCV)*, Seoul, South Korea, 2019, pp. 7314–7323.

[13] H. Sun *et al.*, "Spatial-frequency residual-guided dynamic perceptual network for remote sensing image haze removal," *IEEE Trans. Geosci. Remote Sens.*, vol. 63, pp. 1–18, 2025, doi: 10.1109/TGRS.2025.3543728.

[14] H. Sun, S. Li, B. Du, L. Zhang, D. Ren, and L. Tong, "Dynamic-routing 3D-fusion network for remote sensing image haze removal," *IEEE Trans. Geosci. Remote Sens.*, vol. 63, pp. 1–15, 2025, doi: 10.1109/TGRS.2025.3526993.

[15] N. Wang, Z. Cui, Y. Su, Y. Lan, Y. Xue, C. Zhang, and A. Li, "Weakly supervised image dehazing via physics-based decomposition," *IEEE Trans. Circuits Syst. Video Technol.*, vol. 36, no. 1, pp. 637–652, Jan. 2026, doi: 10.1109/TCSVT.2025.3596024.

[16] Y. Su, N. Wang, Z. Cui, Y. Cai, C. He, and A. Li, "Real scene single image dehazing network with multi-prior guidance and domain transfer," *IEEE Trans. Multimedia*, vol. 27, pp. 5492–5506, 2025, doi: 10.1109/TMM.2025.3543063.

[17] L. Zhu, Y. Su, Z. Cui, Y. Lan, N. Wang, L. Zhang, and Y. Cai, "Diffusion models and its applications in image dehazing: A survey," *IET Image Process.*, vol. 20, no. 1, Jan. 2026.

[18] J. Chen, X. Yan, Q. Xu, and K. Li, "Tokenize image patches: Global context fusion for effective haze removal in large images," in *Proc. IEEE/CVF Conf. Computer Vision and Pattern Recognition (CVPR)*, Nashville, TN, USA, 2025, pp. 2258–2268.

[19] Y. Cui, W. Ren, X. Cao, and A. Knoll, "Revitalizing convolutional network for image restoration," *IEEE Trans. Pattern Anal. Mach. Intell.*, vol. 46, no. 12, pp. 9423–9438, Dec. 2024.

[20] Z. Chen, Z. He, and Z.-M. Lu, "DEA-Net: Single image dehazing based on detail-enhanced convolution and content-guided attention," *IEEE Trans. Image Process.*, vol. 33, pp. 1002–1015, 2024.

[21] L. Ma *et al.*, "CoA: Towards real image dehazing via compression-and-adaptation," in *Proc. IEEE/CVF Conf. Computer Vision and Pattern Recognition (CVPR)*, Nashville, TN, USA, 2025, pp. 11197–11206.

[22] S. C. Huang, T. H. Le, and D. W. Jaw, "DSNet: Joint semantic learning for object detection in inclement weather conditions," *IEEE Trans. Pattern Anal. Mach. Intell.*, vol. 43, pp. 2623–2633, 2021.

[23] W. Y. Liu *et al.*, "Image-adaptive YOLO for object detection in adverse weather conditions," in *Proc. AAAI Conf. Artificial Intelligence*, 2022, pp. 1792–1800.

[24] K. Hu, F. Wu, Z. F. Zhan, J. Luo, and H. Y. Pu, "High-low level task combination for object detection in foggy weather conditions," *J. Vis. Commun. Image Represent.*, vol. 98, p. 8, 2024.

[25] Y. Z. Wang *et al.*, "TogetherNet: Bridging image restoration and object detection together via dynamic enhancement learning," *Comput. Graph. Forum*, vol. 41, pp. 465–476, 2022.

[26] H. Zhang, S. Wen, Z. Wei, and Z. Chen, "High-resolution feature generator for small-ship detection in optical remote sensing images," *IEEE Trans. Geosci. Remote Sens.*, vol. 62, pp. 1–11, 2024, Art. no. 5617011.

[27] Y. Li, Q. Ling, Y. An, H. Yin, and X. Zhang, "DHC-Net: A remote sensing object detection under haze and class imbalance," *IEEE Trans. Geosci. Remote Sens.*, vol. 63, pp. 1–16, 2025.

[28] C. Feng, Z. Chen, X. Li, C. Wang, J. Yang, M.-M. Cheng, Y. Dai, and Q. Fu, "HazyDet: Open-source benchmark for drone-view object detection with depth-cues in hazy scenes," arXiv:2409.19833, 2024.

[29] W. Lu, S.-B. Chen, H.-D. Li, Q.-L. Shu, C. H. Q. Ding, J. Tang, and B. Luo, "LEGNet: A lightweight edge-Gaussian network for low-quality remote sensing image object detection," arXiv:2503.14012, 2025.

[30] Y. Wan, J. Li, L. Lin, H. Li, Q. Yuan, C. Zeng, and Y. Yang, "DFI-FODN: Dehazing feature injected foggy image object detection network under multi-task learning framework," in *Proc. IEEE Int. Geosci. Remote Sens. Symp. (IGARSS)*, 2025, pp. 8462–8465, doi: 10.1109/IGARSS55030.2025.11243574.

[31] Z. Zhang, J. Li, Y. Liang, J. Yan, Y. Xiao, X. Su, and Q. Yuan, "ECRformer: An efficient cloud removal Transformer with semantic-decoupled learning for multimodal satellite imagery," *ISPRS J. Photogramm. Remote Sens.*, vol. 237, pp. 323–338, 2026, doi: 10.1016/j.isprsjprs.2026.04.009.

[32] Z. Zhang, J. Yan, Y. Liang, J. Feng, H. He, and L. Cao, "Multiscale restoration of missing data in optical time-series images with masked spatial-temporal attention network," *IEEE Trans. Geosci. Remote Sens.*, vol. 63, pp. 1–15, 2025, doi: 10.1109/TGRS.2025.3574799.

[33] Z. Liu, T. Fang, H. Lu, W. Zhang, and R. Lan, "MASFNet: Multi-scale adaptive sampling fusion network for object detection in adverse weather," *IEEE Trans. Geosci. Remote Sens.*, vol. 63, pp. 1–15, 2025, doi: 10.1109/TGRS.2025.3558541.

[34] T. Y. Lin *et al.*, "Feature pyramid networks for object detection," in *Proc. IEEE/CVF Conf. Computer Vision and Pattern Recognition (CVPR)*, Honolulu, HI, USA, 2017, pp. 936–944.

[35] S. Chen, P. Sun, Y. Song, and P. Luo, "DiffusionDet: Diffusion model for object detection," in *Proc. IEEE/CVF Int. Conf. Computer Vision (ICCV)*, 2022, pp. 19773–19786.

[36] H. Rezatofighi, N. Tsoi, J. Gwak, A. Sadeghian, I. Reid, and S. Savarese, "Generalized intersection over union: A metric and a loss for bounding box regression," arXiv:1902.09630, doi: 10.48550/arXiv.1902.09630.

[37] I. Loshchilov and F. Hutter, "Decoupled weight decay regularization," arXiv:1711.05101, doi: 10.48550/arXiv.1711.05101.

[38] G. S. Xia *et al.*, "DOTA: A large-scale dataset for object detection in aerial images," in *Proc. IEEE/CVF Conf. Computer Vision and Pattern Recognition (CVPR)*, Salt Lake City, UT, USA, 2018, pp. 3974–3983.